Journal of Alloys and Compounds 786 (2019) 570–580

Contents lists available at ScienceDirect

Journal of Alloys and Compounds

journal homepage: http://www.elsevier.com/locate/jalcom

Microstructure, mechanical and wear properties of the A357 composites reinforced with dual sized SiC particles

Avinash Lakshmikanthan [a, b], Srikanth Bontha [a, *], M. Krishna [c], Praveennath G. Koppad [d], T. Ramprabhu [e]

[a] Department of Mechanical Engineering, National Institute of Technology Karnataka, Surathkal, Mangaluru 575025, India
[b] Department of Mechanical Engineering, Nitte Meenakshi Institute of Technology, Bengaluru 560064, India
[c] Department of Mechanical Engineering, RV College of Engineering, Bengaluru 560059, India
[d] Department of Mechanical Engineering, Dayananda Sagar College of Engineering, Bengaluru 560078, India
[e] CEMILAC, Defence R&D Organization, Bangalore 560093, India

ARTICLE INFO

Article history:
Received 3 October 2018
Received in revised form
25 January 2019
Accepted 31 January 2019
Available online 1 February 2019

Keywords:
Dual particle size (DPS) composites
Stir casting
Microstructure
Mechanical properties
Wear

ABSTRACT

Current work reports on the development of A357 alloy composite which is reinforced with dual size SiC particles by stir casting route. Influence of different weight fractions (3% coarse+ 3% fine, 4% coarse + 2% fine, and 2% coarse + 4% fine) of dual size SiC particles on mechanical properties and wear resistance of A357 composites is the focus of this work. Hardness and tensile properties were studied for dual size composites and then were compared with A357 alloy. Microstructural study, fractured surface and worn surface investigation were carried out using optical and scanning electron microscopes respectively. Microstructural analysis showed fairly uniform dispersion of dual size SiC particles in A357 matrix with good interfacial bonding. Compared to A357 alloy, the composites showed improvement in hardness, yield, and tensile strength. In particular, composite with 4 wt. % of fine and 2 wt. % of large SiC particles displayed the highest tensile strength while composite with 4 wt. % of large and 2 wt. % of fine SiC particles exhibited high hardness and wear resistance among A357 alloy and dual particle size composites. The strengthening mechanisms that contributed to improvement in strength values were effective load transfer and dislocation strengthening due to thermal mismatch.

1. Introduction

In the past few decades, there has been a lot of research devoted to the development of low cost and lightweight metal matrix composites. In this regard, aluminium and its alloys having low density were being used as matrix materials with several carbon and ceramic particulates as reinforcement materials for various applications pertaining to automotive, aerospace and construction industries [1–5]. In particular, Al-Si based A357 alloy possesses excellent castability, weldability, good mechanical properties, and corrosion resistance. Due to these characteristics, this alloy is the prime candidate material for automotive and aeronautical components [6]. Most of the components are fabricated by the casting process, and the resulting as-cast microstructure decides the physical and mechanical properties. Carbon and ceramic-based reinforcements are used to improve the mechanical, tribological and physical properties of A357 alloys. The reinforcements like graphite fiber (P-55) [7], carbon fiber bundles (K139) [8] and SiC particles [9,10] were used to reinforce A357 aluminium alloy. Especially SiC is the most commonly used reinforcement for A357 aluminum alloy compared to others. Bloyce and Summers [9] reported the static and dynamic properties of A357-SiC composites fabricated by squeeze-casting technique. Along with a homogenous microstructure, significant improvements in both the tensile strength and elongation were observed. The outcome of this is already seen in the development of brake drums, cylinder heads, connecting rods and engine blocks. Aluminium reinforced with Al_2O_3 and SiC was used to fabricate automotive components like valve spring retainers and fuel pump pushrods [11]. The developed composite was found to be stiffer and 30% lighter than 4130 steel. The benefits from these properties were higher engine rpm's, improved damping characteristics and increased horsepower. For thermal management applications, aluminium reinforced with carbon fiber, SiC and diamond are quite popular, as they possess

* Corresponding author.
E-mail address: srikanth.bontha@nitk.edu.in (S. Bontha).

https://doi.org/10.1016/j.jallcom.2019.01.382
0925-8388/

high thermal conductivity and tailorable thermal expansion coefficient. With the usage of such composites, it was observed that the heat dissipation was quite effective and had minimum thermal stresses necessary for component performance and life cycle [12]. The latest modification done to the metal matrix composite is usage of dual particle size reinforcements for better wear resistance and tailoring the coefficient of thermal expansion according to the requirements. The idea behind using dual size reinforcements is that, coarse size reinforcement helps in improving the hardness, fracture toughness and wear resistance, while the finer size reinforcement helps in improving mechanical properties like tensile strength and ductility [13–15]. Bindumadhavan et al. [16] studied the effect of dual particle size on mechanical and wear properties of Al-Si-Mg composites and compared the same with single particle reinforced composite. The average particle size of SiC used for dual particles size composite were 47 and 120 μm. Compared to single particle size, dual particle size composite exhibited better wear resistance and impact energy. Wang et al. [17] studied the microstructure and thermo-mechanical properties of dual particle size SiC reinforced A356 composites prepared by pressure less infiltration. The microstructures showed clear edges of SiC indicating absence of any particle damage due to the process. Further, the absence of pores showed good bonding mechanism. The bending strength of composites was found to increase with decrease in particle size while thermal conductivity dropped due to interfacial heat barrier and presence of Fe impurities. Kumar et al. [18] studied the effect of coarse (106–125 μm) and fine (20–32 μm) zircon particles on wear behavior of LM13 composites. The stir cast composites were subjected to wear test by keeping sliding distance and velocity constant while the load was varied. The composite with 3% fine and 12% coarse zircon showed less wear resistance than that of composite with 3% coarse and 12% fine zircon particles. This was attributed to shielding of fine zircon particles and wear resistance offered by coarse ones during wear test. On the other hand, Montoya-Dávila et al. [19] in their work studied the hardness and fracture toughness of Al-SiC composites with three different particle sizes (10, 68 and 140 μm) that were prepared using infiltration process. All the properties showed significant improvement with increase in size distribution. The increase in the fracture toughness was mainly attributed to better bonding between Al and SiC leading to effective load transfer.

Literature reviewed above suggests that strength and wear resistance of aluminium and its alloys can be increased by using dual particle size reinforcement in proper proportion. The effect of dual particles size on the mechanical and wear behavior of the composites is not yet studied systematically. Notably, the question of what ratio of coarse and fine size particles is optimal to improve the mechanical and tribological properties of the composites has not yet been addressed. To this end, the focus of the present work is to investigate the effect of the addition of SiC with two different particle sizes (140 ± 10 μm and 30 ± 5 μm) on the mechanical and tribological properties of an A357 alloy matrix.

2. Experimental procedures

2.1. Materials

A357 alloy was selected as the matrix material due to its industrial importance. The chemical composition of as-cast A357 alloy is given in Table 1. Silicon carbide with two different particle sizes of 140 ± 10 μm (coarse) and 30 ± 5 μm (fine) was used as a reinforcement material.

2.2. Composite fabrication

The melt-stirring assisted permanent mold die casting technique was adopted to fabricate the A357 alloy DPS composites. A novel two-step mixing technique, right selection of stirrer speed, particle preheating, and degassing using Hexachloroethane tablets (C_2Cl_6) have helped to overcome the limitation in achieving uniform dispersion of ceramic particles [20–25]. The A357 alloy in the form of ingot was initially placed inside a crucible made up of graphite and superheated to 800 °C in a resistance-heated furnace (230 V, 2 kW Power). To minimize casting defects such as voids, porosity and blow holes formed, the molten metal was degassed using commercially available Hexachloroethane tablets (C_2Cl_6). The SiC particles of both sizes ((140 ± 10 μm (L) and 30 ± 5 μm (S))) were preheated to 1100 °C for 2 h to remove moisture, residues and loose scales. The molten metal was stirred using a motorized stirrer operated at 550–600 rpm to create a vortex. In order to avoid any contamination, the mechanical stirrer made up of chromium steel blades was coated with zirconium. The total weight percentage of coarse and fine SiC particles is kept at 6 wt. % in all the composites considered in this work. These particles are introduced to the melt vortex at a rate of 15–20 g/minute using a funnel. The stirring was continued for about 15 min at a low speed of 300 rpm to ensure proper dispersion of SiC particles. The composite melt was finally poured into a pre-heated cast iron mold by maintaining a pouring temperature of 730 °C and then allowed to solidify at ambient temperature. The experimental set up of stir casting and its process details are given in Fig. 1 and Table 2 respectively.

Three different composites with varying SiC percentages namely, DPS1 (3% Large SiCp+ 3% Small SiCp), DPS2 (4% Large SiCp+ 2% Small SiCp) and DPS3 (2% Large SiCp+ 4% Small SiCp) were fabricated to arrive at optimum combination of particle size and content. A357 alloy without any reinforcement was also cast for comparison purposes. The reinforcement combination dual particle size composites are given in Table 3.

2.3. Metallographic studies

The specimens were prepared as per standard metallurgical procedures for microstructure analysis. The samples were etched with Keller's reagent. The highly polished surfaces were observed under Optical microscope (Model: Nikon LV150). The fractured surfaces after tensile testing, wear surface morphology after wear testing of A357 alloy and its composites were studied using a scanning electron microscope (Model: TESCAN Vega 3 LMU) with an EDS attachment.

2.4. Vickers hardness test

The hardness test was carried out using a Micro Cum Macro-Vickers hardness testing machine (Model: VH1150) as per ASTM E384 standards. A Vickers hardness tester having a standard rectangular pyramid diamond indenter ($136^0 \pm 0.5^0$) was used to apply

Table 1
Chemical composition of A357.

Elements	Si	Mg	Fe	Cu	Mn	Ti	Zinc	others	Al
Wt. %	7.398	0.540	0.086	0.017	0.024	0.177	0.003	0.073	Balance

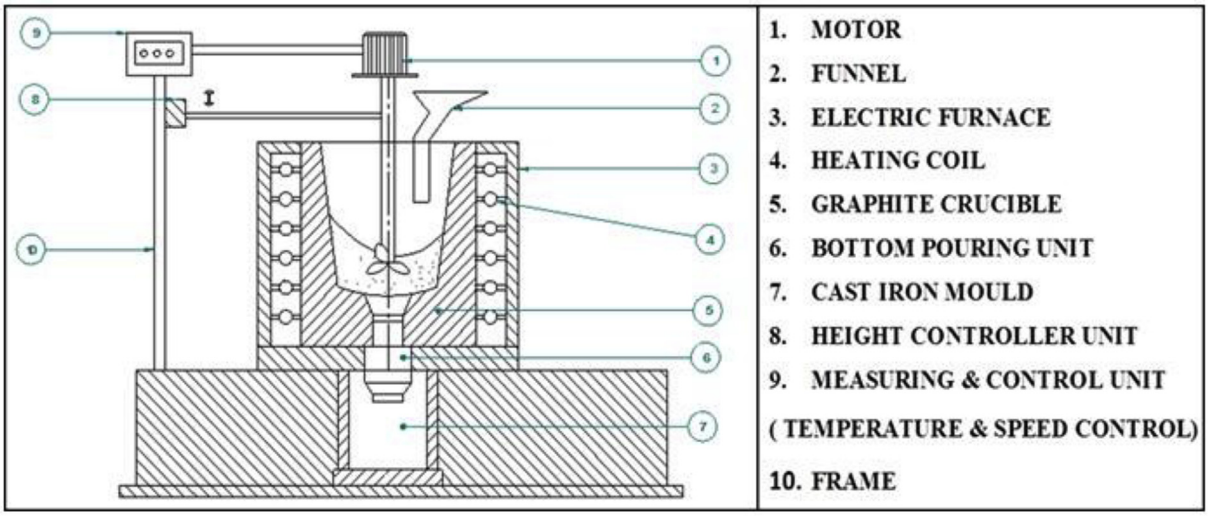

Fig. 1. Stir casting Setup (Bottom Pouring Technique).

Table 2
Parameters used in Stir Casting Process.

Pouring Temperature	Stirring Duration	Stirring Speed	Stirrer Position	Impeller
730 °C	~15 min	550–600 rpm	~2/3″ depth from the bottom of crucible	Zirconium coated chromium steel, 3 blade fan type

Table 3
Reinforcement combination of DPS Composites.

S/No	Composition of Composite Base alloy (%)	Amount of Reinforcement Wt. %	Coarse Size SiC Particles (140 ± 10 μm)	Fine Size SiC Particles (30 ± 5 μm)	Designation
1	100	0	0	0	A357 alloy
2	94	6	3	3	DPS1
3	94	6	4	2	DPS2
4	94	6	2	4	DPS3

a load of 5 kgf for about 10 s.

2.5. Tensile test

Tension test specimens were machined as per ASTM E8M-15a standards and then were tested at room temperature using a universal testing machine (Model: TUE-C-400). Tension test was conducted at a strain rate of 0.2 mm/s. The strength and ductility values reported here in were based on an average of five measurements.

2.6. Wear test

Dry sliding friction and wear tests were conducted using Pin-on-Disc machine (Model TR-20LE, Ducom make) as per ASTM-G99 standards. The specimens were ground to obtain a surface finish of 0.2 ± 0.05 μm (Ra). The counterface disc used is made up of En-32 steel disc of 160 mm diameter and 8 mm thickness with a hardness value of HRC65. The composition of counterface disc is given in Table 4.

The test was conducted at ambient room temperature of 26 °C and at a relative humidity condition of 35–40% RH respectively. Load was varied from 10 N to 30 N at a sliding velocity of 2.5 m/sec and sliding distance of 1500 m. For each parameter, an average of 3 measurements are reported.

3. Results and discussion

3.1. Microstructure

Fig. 2 (a) and (b) show optical micrographs of as cast A357 alloy at low (100X) and high (500X) magnifications respectively. The micrographs reveal two phases: primary α-Al phase, Al-Si eutectic. The solid solubility of Si in Al is 1.65 wt. % at 577 °C. The solid solution of Al and Si consists of α-Al grains with dendritic grain structure. Solidification of Al alloy starts with the formation of primary α-Al phase. The dendritic structure formation is decided by the type of nucleation, the cooling rate and the undercooling temperature range. In the present case, solidification is a slow process. Nucleation preferably starts heterogeneously at Ti nucleants, the mold wall, and SiC particles. When the alloy solidifies, it

Table 4
Chemical composition of En-32 steel disc.

Elements	C	Si	Mn	S	P	Ni	Cr	Mo	Fe
Wt. %	0.14%	0.18%	0.52%	0.015%	0.019%	0.13%	0.05%	0.06	Balance

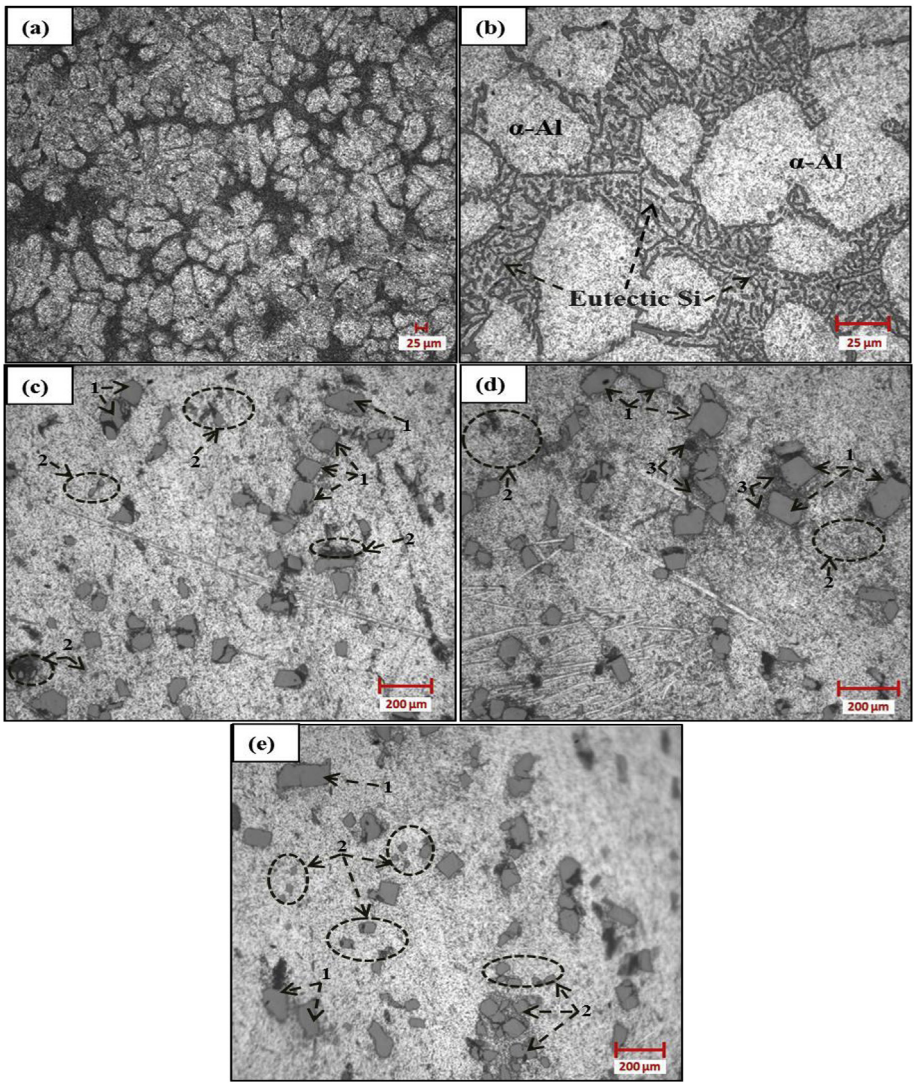

Fig. 2. Optical micrographs of as cast A357 alloy and DPS Composites (a) A357 alloy showing dendritic structure (b) A357 alloy showing interdendritic region (c) DPS1 composite (d) DPS2 composite (e) DPS3 composite. In Fig. 2(c–e), 1 represents Coarse SiCp, 2 represents Fine SiCp, 3 shows clustering of fine SiCp.

forms the α-Al grain primary dendrites. The growth of primary dendrites is retarded by the increase of temperature in the solidification front due to the loss of heat by the cooling, the presence of the second phase particles and the solidification front of the neighbor growing grains primary dendrites. At the same time, undercooling is relatively high in the liquid surrounding the sides of dendrites. This result in the formation of solid branches in the primary dendrites called the secondary dendrites. Hence, the solidification of the composites is driven by the formation of primary and secondary dendritic arms in the liquid. Fig. 2(c) shows optical micrograph of fairly uniform dispersion of both sizes of SiC particles in the DPS1 composite. The distribution of SiC particles is almost homogenous in the DPS1 composite. The particles pin the grain boundary and restrict the grain growth in the present case in addition to acting as the nucleating sites during solidification. The absence of clustering zone in the microstructure implies that the particle distribution is uniform in the composites. The presence of dendrites masks the grain boundary in the composites.

Fig. 2 (d) shows optical micrograph of DPS2 composite consisting of 4 wt. % of large SiC particles and 2 wt. % of fine SiC particles. The microstructure is dominated by large SiC particles with very few fine particles around them. The finer SiCp are pushed at a faster rate during stirring and they are distributed between the larger particles. The interface between the particle and matrix alloy appears to be clean and smooth and hence is the reason for better mechanical and wear properties. This is because the load transfer occurs through the interface [26–28].

Fig. 2 (e) shows the optical micrograph of DSP3 composite which consists of 4 wt. % fine SiC particles and 2 wt. % of large SiC particles. Although both particles are distributed uniformly, the finer particles have agglomerated and form a network arrangement. This is mainly due to pushing of finer SiC particles by solid-liquid interface during solidification. Overall, the DPS composites show an almost homogenous distribution of dual size SiC particles in alloy matrix. Uniform distribution of particles is desired for achieving better wear behavior and mechanical properties.

Fig. 3 shows EDS of DPS1 composite exactly on SiC particle to confirm that these are SiC particles and not eutectic silicon. The purpose behind taking EDS on SiC particle is that in many cases the presence of reinforcements can cause refinement of eutectic silicon

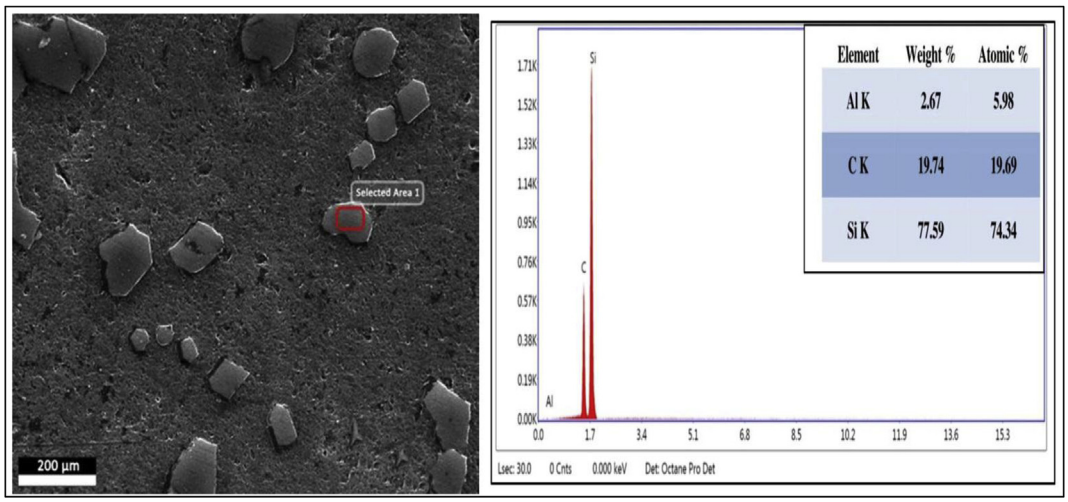

Fig. 3. EDS spectra taken on DPS1 composite confirming the presence of SiCp.

along with the microstructure [29]. It was necessary to do EDS to confirm that the particles seen in SEM micrographs are SiC particles.

3.2. Vickers hardness

Fig. 4 shows the variation of the hardness of A357 alloy and DPS composites. Compared to the as-cast alloy, the DPS1, DPS2, and DPS3 composites showed an increment of 9.42%, 15.13% and 5.83% increment in hardness respectively. Among the DPS composites, the DPS2 composite with 4 wt. % of large SiC particles and 2 wt. % of fine SiC particles shows slightly higher hardness. This may be due to the higher amount of large size SiC particles uniformly dispersed in the matrix compared to smaller size SiC particles as shown in Fig. 2(d). The higher amount of coarser particles in composites shields the finer particles; Further, coarser particles help to carry a more significant portion of the applied load compared to the finer particles [16].

Compared to the large size particles, the small size particles are more prone to the particle clustering [30]. Hence, the dispersion of small size particles is very difficult. The improvement in hardness values of the DPS composites are attributed to the following factors: (1) Dispersion of hard ceramic particles (SiC) in a soft ductile matrix leading to hardening of the matrix, (2) Particle strengthening of the composites through dislocation density strengthening and plastic strain constraint effects and (3) grain refinement of the matrix by SiC particles and primary Si particle refinement [30–36].

3.3. Tensile strength

It can be observed from Fig. 5 that, addition of dual size SiC particles has enhanced the strength (UTS and YS) of all composites. The percent increase of tensile strength of DPS1, DPS2, and DPS3 composites are 40.98%, 37.61%, and 45.30% respectively when compared to the as-cast A357 alloy. Similarly, the percent increase of the yield strength of DPS1, DPS2, and DPS3 composites is 67.64%, 53.48%, and 76.33% respectively when compared to the as-cast A357 alloy. Among the DPS composites, the DPS3 composite with 2 wt. % of large SiC particles and 4 wt. % of fine SiC particles shows slightly higher tensile and yield strength. This may be due to the higher amount of fine size particles almost uniformly distributed in the matrix compared to larger size SiC particles.

The addition of SiC particles helps to refine the primary Si in the Al-Si alloy by grain refinement through the nucleant site and particle grain pinning effects. The refinement of primary Si leads to the short fibrous shape Si in the composites, as seen in Fig. 2(c–e). The refinement of Si particles improves the tensile properties by restoring the ductility. Also, the fine Si particles improve the strength by acting as a second phase. The SiC particles improve the tensile properties by three dominant processes: (1) grain refinement and primary Si particles refinement, (2) load transfer effect and (3) dislocation strengthening and plastic strain constraint effects [33,34]. The thermal expansion and elastic modulus mismatch between the matrix and the particles generates dislocations around the particles and increases the dislocation density. The increase in

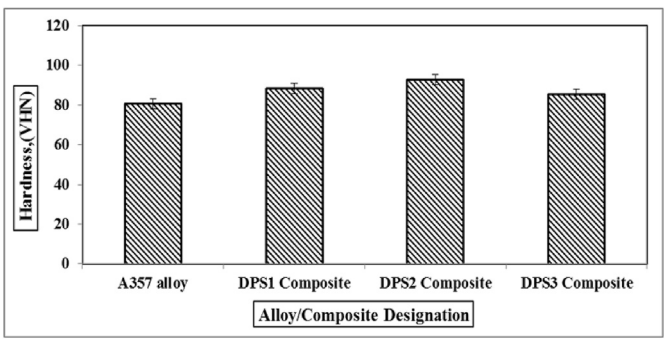

Fig. 4. Variation of the hardness of A357 alloy and DPS composites.

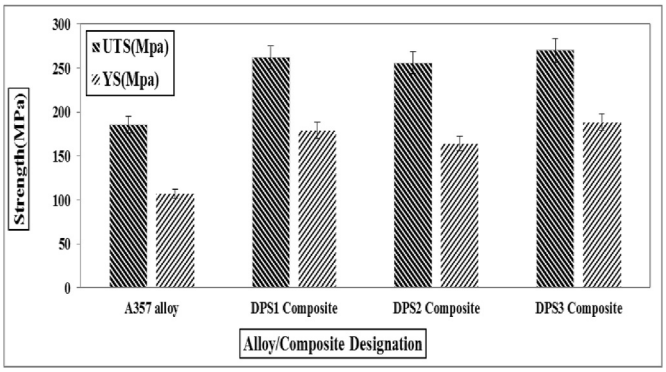

Fig. 5. Variation of tensile strength values of A357 alloy and DPS Composites.

dislocation density enhances the strength of the composites (dislocation strengthening). Also, the strain in the matrix is localizied due to the non-deforming SiC particles during the deformation, which causes strengthening through local plastic constraint [37]. The hard and stiff SiC particles act as load bearing elements in the composites and enhance the strength. As explained earlier, the SiC particles enhance the grain refinement through the nucleation site and grain boundary pinning effects. The Hall-Pitch relation explains the strength improvement though the decrease of matrix grain size [37].

The variation in ductility of A357 alloy and its composites is shown in Fig. 6. The reduction in ductility for DPS1, DPS2 and DPS3 composites is about 21.83%, 22.41% and 18.12% respectively when compared to that of A357 alloy. It is observed that the inclusion of dual size SiC particles in A357 alloy has resulted in significant loss of ductility. This is because, the presence of hard SiC particles will act as barrier to the dislocation motion during tensile loading. These results are in good agreement with those reported in literature [38].

3.4. Tensile fracture analysis

Fig. 7(a–d) show the SEM images of fractured surfaces of A357 alloy and DPS composites after the tensile test. The A357 alloy exhibits a typical intercrystalline fracture as shown in Fig. 7 (a). The fracture is mainly due to the presence of dendritic shrinkage porosity. The crack nucleation takes place at these dendritic shrinkage porosity regions and propagates along these dendrites causing failure of A357 alloys. However, the porosity in the casting is also influenced by the formation of dendritic structure. On the other hand, all the DPS composites showed brittle failure along with quasi-cleavage fracture, as shown in Fig. 7 (b) – (d). The quasi-cleavage fracture is generally seen in materials with lower elongation values. This can be due to breaking of Al-Si eutectic particles or large SiC particles. It is well known that the particle size and shape have huge influence on the tensile properties. The large and elongated Al-Si eutectic particles present in the A357 alloy are more prone to cracking. So, in case of A357 alloy, the inter-dendritic cracking and cracking of silicon particles dominate the fracture process. While in the case of composites, the dislocations pile-up at the vicinity of SiC particles giving rise to stress fields which in turn cause the local fluctuations leading to cracking of SiC particles. It is important to note that the good bonding between A357 matrix and SiC particles has resulted in breaking of SiC particles during tensile loading rather than particle debonding. In case of tensile loading, the interfacial bonding between the SiC particles and A357 matrix plays an important role. If the interfacial bonding is good, then it tries to retain the SiC particles in the matrix during loading conditions. But, as the load increases, due to high interfacial bonding, the SiC particles get fractured rather than debonding. Hence, in case of composites, the nature of fracture is brittle and quasi cleavage feature mode [39,40].

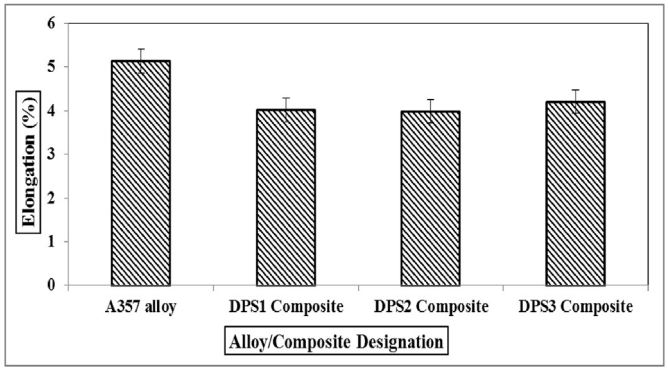

Fig. 6. Variation of % elongation values of A357 alloy and DPS Composites.

3.5. Wear behavior

The graphical interpretation of wear rate for A357 alloy and DPS2 composite is shown in Fig. 8 (a–d) for different loads. It can be observed that for A357 alloy, the wear rate is increasing linearly for both 10 and 30 N loads. However, in the case of 30 N applied load, there is rapid increase in wear rate of A357 alloy as shown in Fig. 8 (b). The degree of fluctuation is quite high in this case particularly at 350 s for 10 N and 270 s for 30 N loads indicating seizure phenomena taking place. In case of DPS2 composite, the wear rate is not as high as that of A357 alloy as seen in Fig. 8 (c) & (d) for 10 N and 30 N respectively. The degree of fluctuation is smaller for DPS2 composite when compared to that of A357 alloy indicating high seizure resistance. This is the reason why a steady state regime without any notable fluctuations is observed in the A357 alloy which can be attributed to prohibition of direct contact between the two mating surfaces by the presence of dual size SiC particles in this composite. In addition to this, the strain hardening effect due to the presence of SiC particles also contributes to lower wear rate values for composites at both lower and higher loads when compared to A357 alloy under similar conditions [41–43].

Fig. 9 shows the effect of applied load on the wear resistance of the A357 alloy and DPS composites. From the figure, it can be observed that DPS composites have higher wear resistance than that of as cast alloy at all load conditions. In particular, DPS2 composite has the least wear rate among all DPS composites considered. From the above figure, it is also observed that up to a load of 20 N, the wear rate increases. With increase in load from 20 N to 25 N, the wear rate stabilizes and with any further increase in load beyond 25 N, wear rate increases rapidly and enters into the severe wear regime. This trend is similar for all the DPS composites and A357 alloy. The A357 alloy displayed highest wear rate for all load conditions which is mainly due to direct metal to metal contact. The increase of wear loss with an increase of load is attributed to several factors such as: (1) higher sub surface deformation and consequent delamination wear, (2) easier removal of load bearing particles, (3) increase of friction due to the higher contact couple surface asperities interlocking, (4) material softening and the matrix oxidation through the friction induced temperature rise, and (5) faster generation and removal of tribolayer. With an increase of load, more factors act alongside resulting in high acceleration of wear rate above the critical load [14,36,44–46].

3.6. Worn surface analysis

Fig. 10 shows the SEM micrographs of wear surface morphology of A357 alloy and DPS composites. One of the common feature observed in the DPS composites is the formation of grooves and ridges running parallel to the sliding direction. The wear surface morphology of the as cast alloy at 10 N and 30 N are as shown in Fig. 10 (a) and (b). The micrographs showed extensive ploughed surface with abrasive grooves which appear deeper and broader. These cavities are formed by delamination wear. With the progress of sliding, these cracks propagate towards the surface along the sliding direction. During the propagation, they branch out and rejoin to cover a large area. Once they reach the surface, they are plowed out as delaminated wear sheets. This observation supports that the delamination wear is more dominant than abrasive wear in the A357 alloy. Further, with the increase in load, the worn surface has wider grooves and larger cavities indicating substantial amount

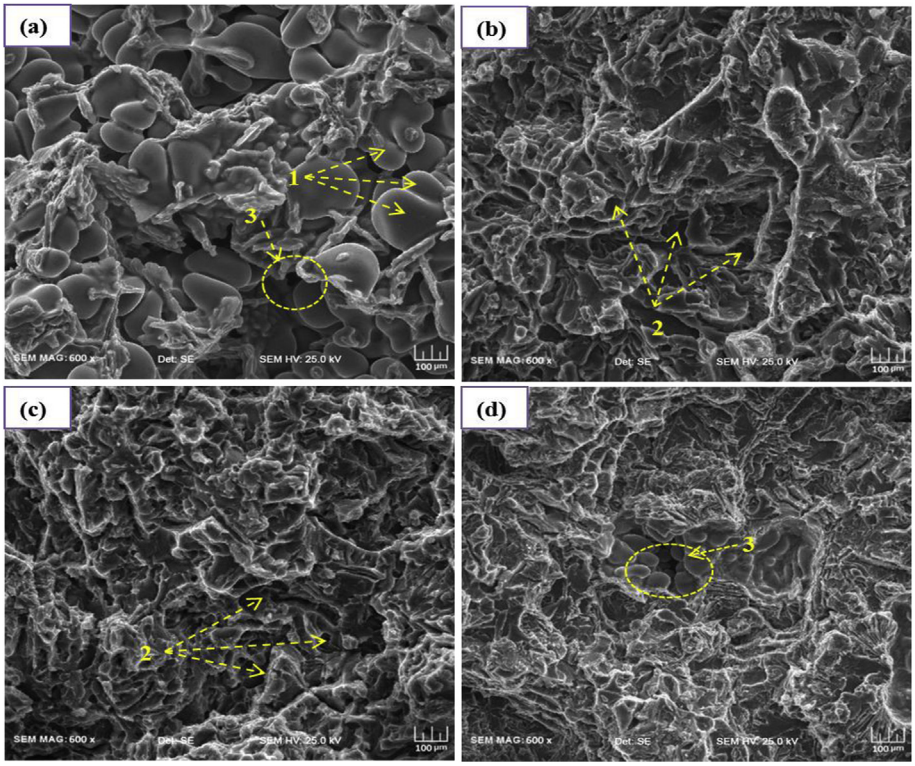

Fig. 7. Fractographs of (a) A357 alloy (b) DPS1 composite (c) DPS2 composite and (d) DPS3 composite. In the figures, 1 represents α-Al grains, 2 represents voids and micro cracks, 3 represents dendritic shrinkage porosity.

of surface material removal. Increase in load applied above 25 N has caused an abrupt rise in A357 alloy wear rate indicating large scale plastic deformation. As the load increases, the hard asperities of counter face penetrate deeper in the soft surface of the alloy. Increasing load results in plastic deformation at the subsurface level resulting in the formation of micro-cracks. These cracks start to coalesce over a period of time during the sliding test in the subsurface region and get detached from the surface. Overall, in case of A357 alloy, worn surface exhibits microgrooves and presence of large cavities in the sliding direction indicating severe plastic deformation of the alloy. These features clearly indicate that the main wear mechanism is delamination wear along with contribution from oxidative wear [47]. Fig. 10 (c) and (d) show the SEM micrographs of wear surface morphology of DPS1 Composite at 10N and 30N respectively. The worn surface is comparatively smooth with shallow ploughing strips; Very small damaged spots in the form of craters can be seen in the DPS1 Composite when compared to A357 alloy. However, DPS2 composite which possesses the lower wear rate exhibits the least extent of grooving, as seen in Fig. 10 (e) and (f) at loads 10 N and 30 N loads respectively. The shallow and thin abrasive grooves running parallel to the sliding direction are mainly seen in the DPS2 composite which is indicative of abrasive wear. This is mainly due to the presence of uniformly dispersed dual size SiC particles which act as load bearing elements. Especially, DPS2 composite has higher weight percentage of large size SiC particles which carry greater portion of load. Further, these large size particles are very effective in reducing the load on the A357 matrix and save the fine size SiC particles from detachment [16]. In addition to this, the strengthening effect of SiC particles enhances the load bearing capacity of the composites by virtue of its high hardness. Further, good interfacial bonding between the SiC particles and A357 alloy plays crucial role in load transfer during sliding test. Further when the load is applied on the A357 alloy during sliding test, the entire load is initially borne by the matrix but in case of composites, the load is transferred from matrix to SiC particles which intern leads to low wear rates [16,48].

Fig. 10 (g) and (h). show the SEM micrographs of wear surface morphology of DPS3 Composite at 10N and 30N loads respectively. The irregular, larger and deeper cavities are seen on the surface of the DPS3 composite. DPS3 composite has higher weight percentage of fine SiC particles when compared to DPS1 composite, and hence the chances of debonding of fine SiC particles from the matrix at higher loads is very high. The width and depth of the grooves increases with the increase in load from 10 N to 30 N which is evident from worn surfaces shown in Fig. 10 (g) and (h). Biswas and Bai [49] have reported that the grooves on the matrix alloy are coarser and smoother in case of composites. It is observed that with an increase in load, the extent of grooving also increases. This can be attributed to the fact that upon increasing load there is an increase in wear rate and also the material gets plastically deformed. EDAX analysis of DPS2 composite as shown in Fig. 11 confirms the presence of Al, Si, C, Fe and O. The presence of Fe clearly indicates the transfer of Fe from the disc (En32) to the worn surface, confirming the formation of mechanically-mixed-layer (MML) on the worn surface of the composite which provides protection to the matrix material. This oxide layer along with material from pin surface creates a mechanically mixed layer which further protects pin surface from any further wear. Thus, the formation of such layers efficiently reduces the wear rate in these composites [50,51].

3.7. Wear debris analysis

The SEM micrographs of wear debris analysis of A357 alloy and DPS composites taken at 10 N and 30 N loads are shown in Fig. 12 (a) – (h). It can be observed that in case of A357 alloy, the wear debris consists of microchips and delamination flakes as shown in

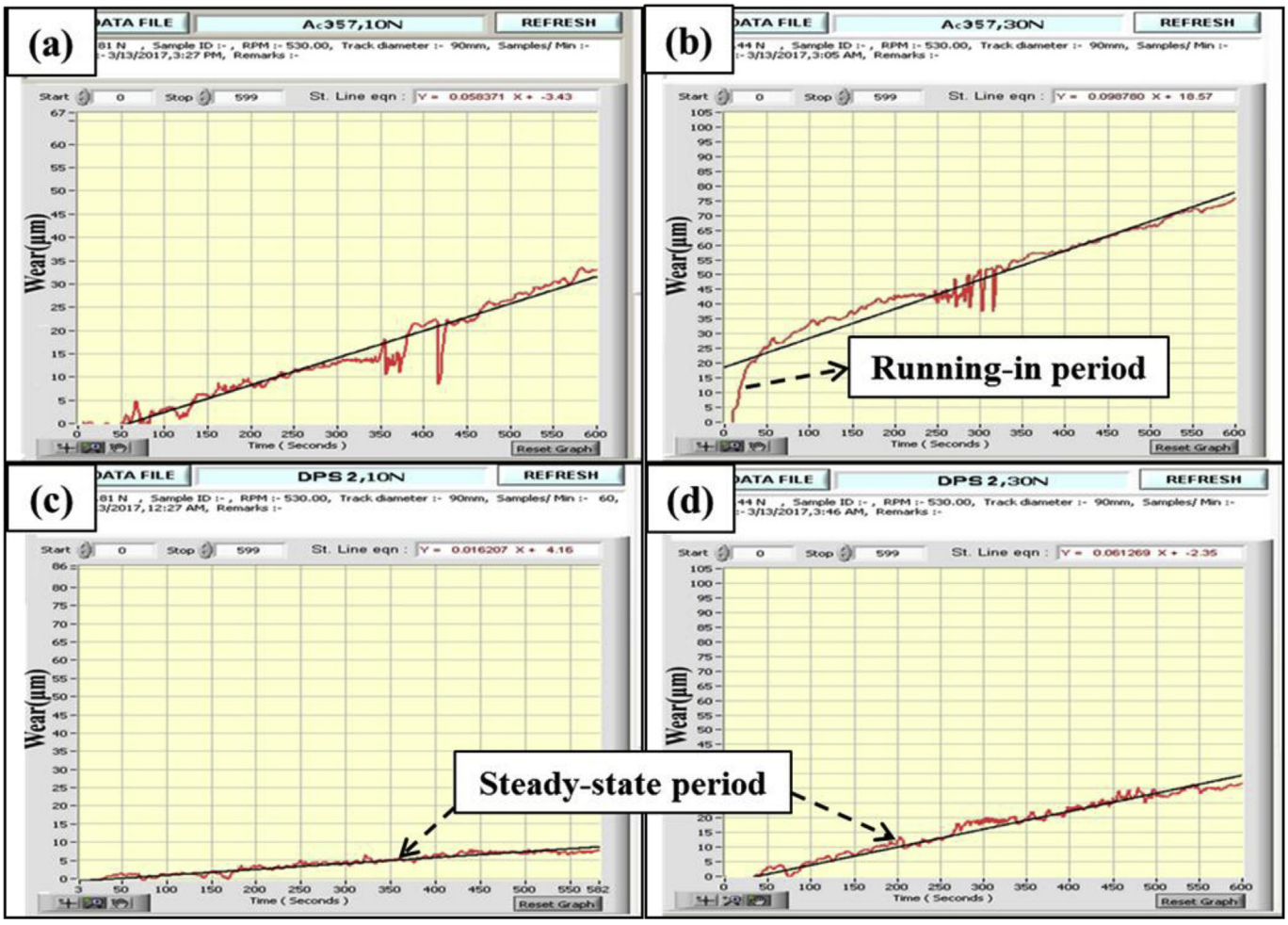

Fig. 8. Graphical interpretation of wear rate for A357 alloy and DPS2 composite (a) A357 alloy at 10N (b) A357 alloy at 30N (c) DPS2 composite at 10N and (d) DPS2 composite at 30N.

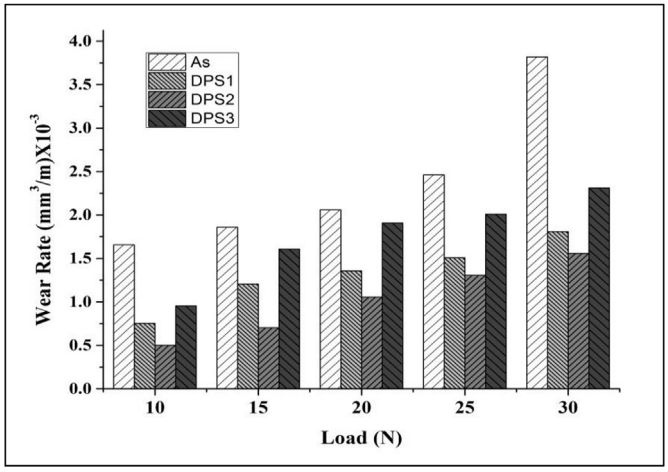

Fig. 9. Effect of load on wear rate (mm^3/m) of A357 alloy and DPS composites. (Sliding Velocity: 2.5 m/s, Sliding distance: 1500 m, load: 10–30 N).

Fig. 12 (a) and (b). But the wear debris taken at 30 N load displayed that size of laminates produced is more than 500 μm while that taken at 10 N load is around 200 μm. Due to continuous sliding, the debris generated showed a layered structure which is quite evident from the SEM micrographs. The increase in load results in severe plastic deformation of alloy surface which interns nucleates the crack in the subsurface level. From the SEM micrograph shown in Fig. 12 (b), it is evident that wear debris of alloy shows presence of numerous cracks on surface adjacent to that of subsurface. These cracks are formed due to accumulation of dislocations due to severe plastic deformation taking place on the surface. In addition to this, the presence of deep micro-grooves on the wear debris clearly explains the material removal due to delamination [52]. These features indicate delamination wear mechanism in oxidative wear conditions. On the other hand, all DPS composites showed flake like morphology and the size and quantity of these flakes increase with the increase in load from 10 N to 30 N. This is mainly due to the fact that at higher loads, the shear force generated is quite larger than that at lower loads leading to larger strain gradient between the two contact surfaces and the interface. Careful examination of wear debris especially in the case of DPS2 composite as shown in Fig. 12 (f) indicates microlevel delamination on flakes of the wear debris which is mainly due to numerous cracks. Further, the debonding of SiC particles from the surface of the composites takes over a period of time during the sliding test. These particles are entrapped in between the two mating surfaces and cause wear grooves. These wear grooves are clearly visible on the surface of the composites as shown in Fig. 12 (d), (f) and (h). Cutting action by the hard asperities and debonded particles cause composite flake generation along

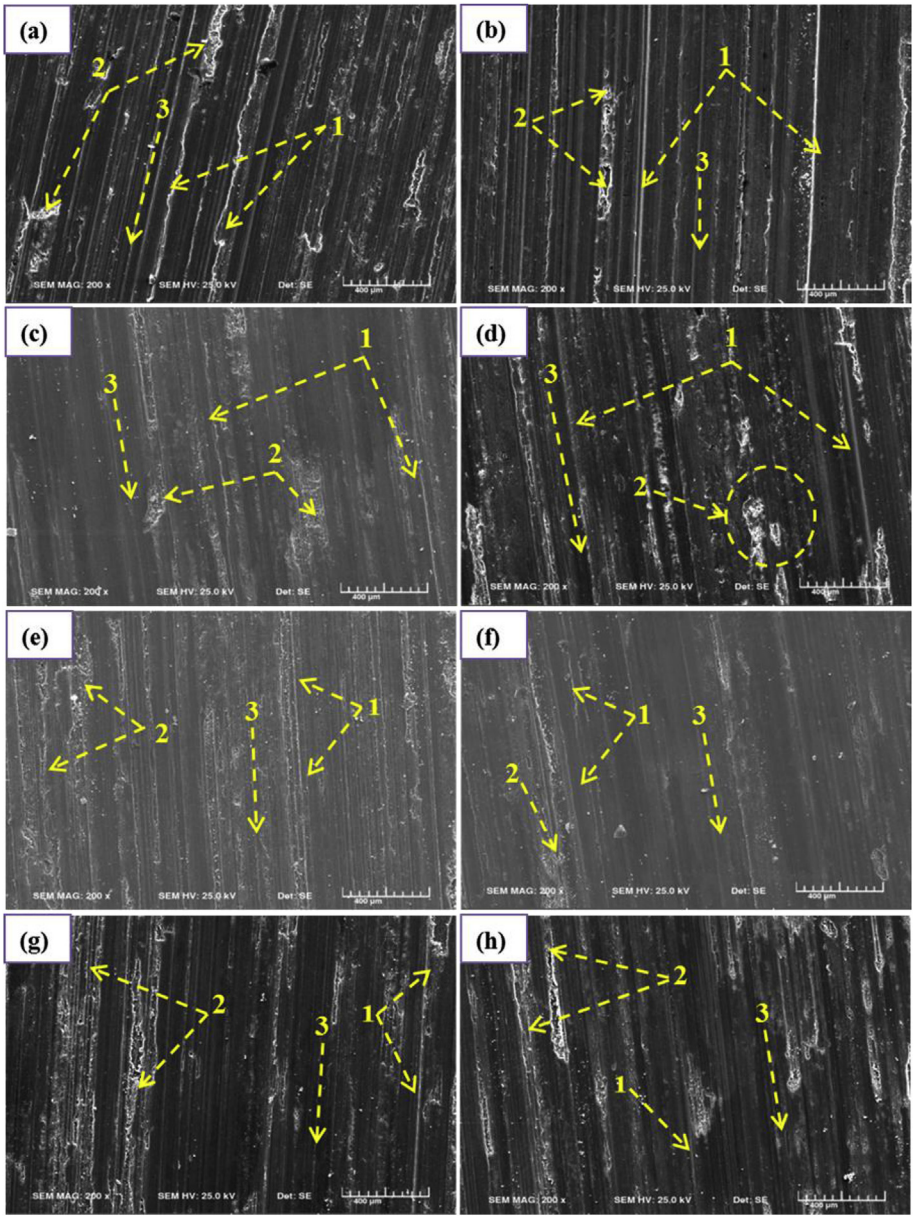

Fig. 10. (a) and (b) SEM of worn surface of A357 alloy (c) and (d) DPS1 composite (e) and (f) DPS2 composite and (g) and (h) DPS3 composite at a loads of 10N and 30N, sliding velocity of 2.5 m/sec and sliding distance of 1500 m. In the figs, 1 represents groove lines, 2 represents delaminated wear sheets and particle pull-out regions and 3 represents sliding direction.

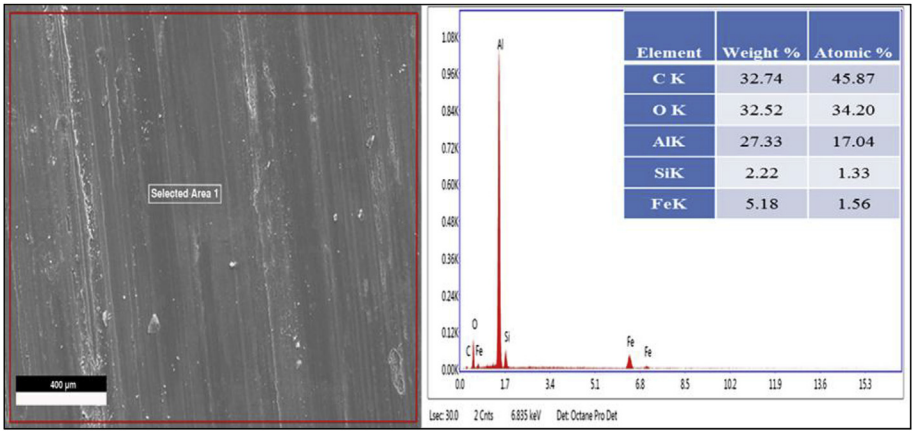

Element	Weight %	Atomic %
C K	32.74	45.87
O K	32.52	34.20
AlK	27.33	17.04
SiK	2.22	1.33
FeK	5.18	1.56

Fig. 11. EDS analysis of selected area on worn surface of DPS2 composite at a load of 30N.

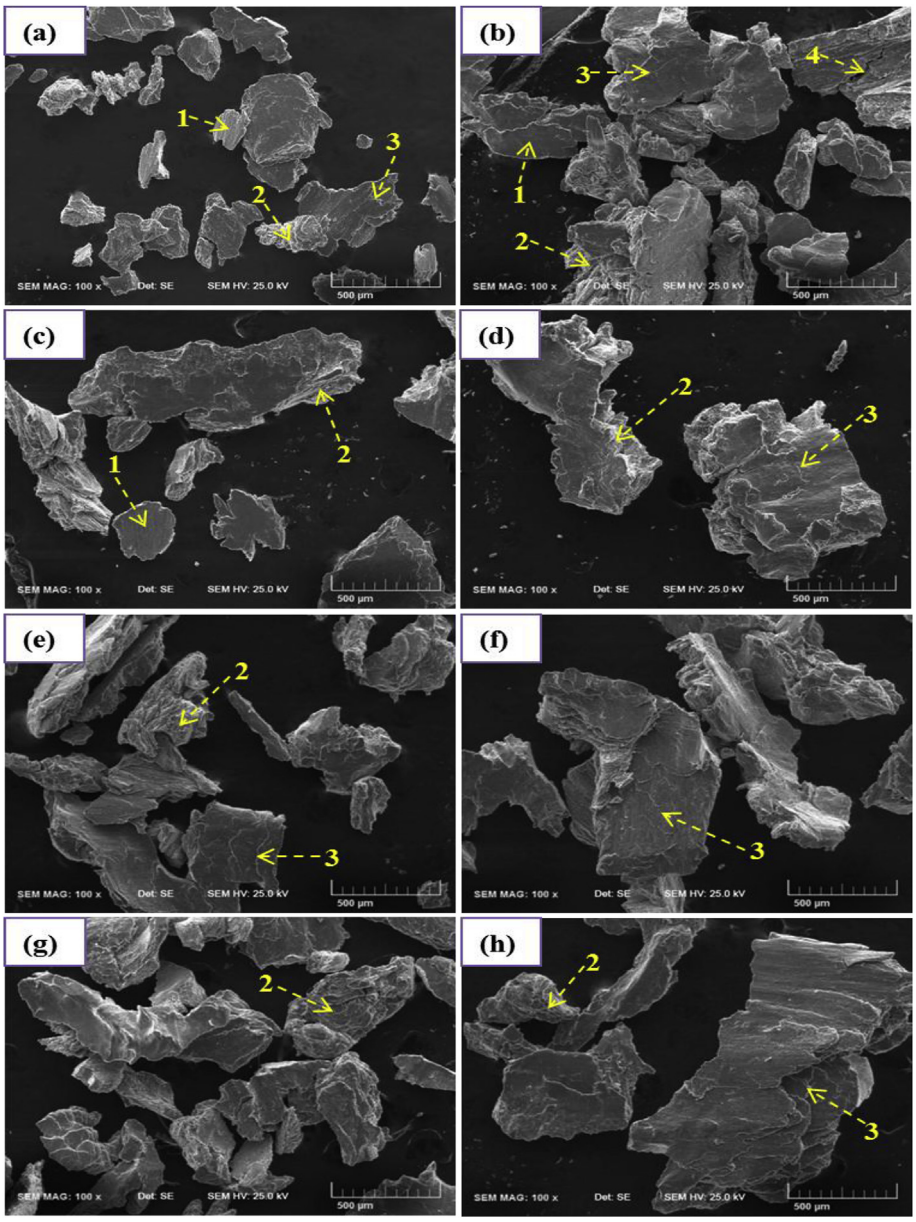

Fig. 12. (a) and (b) SEM images of wear debris of A357 alloy (c) and (d) DSP1composite (e) and (f) DSP2 composite and (g) and (h) DSP3 composite at a loads of 10N and 30N respectively. In the figs, 1 represents scale like debris, 2 represents grooved structured debris, 3 represents curvy pattern debris and 4 represents micro-cracks.

with that of delamination flakes. While in case of DPS3 composite, the flake shows extensive cracks displaying microcutting behavior [53,54].

4. Conclusions

Following conclusions were drawn on dual size SiC reinforced A357 composites developed by stir casting technique.

1. Optical microscopy analysis showed an almost uniform distribution of both smaller and larger SiC particles in the A357 matrix with good interfacial bonding.
2. The hardness studies showed that all composites displayed higher hardness than that of A357 alloy. Among the composites, the one with 4 wt. % of large SiC particles and 2 wt. % of fine SiC particles (DPS2) displays higher hardness value. This is because higher probability for indentation to fall on large hard and stiff particles leads to slightly higher hardness in the DPS2 composite.
3. The yield and tensile strength of all composites were higher than that of the A357 alloy. Among the DPS composites, the one with 2 wt. % of large SiC particles and 4 wt. % of fine SiC particles (DPS3) displayed higher strength. Grain refinement and dislocation strengthening effects by the small size SiC particles and load bearing effect from the large size SiC particles are responsible for higher strength in the DPS3 composite.
4. The wear resistance of all composites was higher than that of the A357 alloy. Load bearing effects and strengthening by dislocation generation and grain refinement are attributed to the higher wear resistance of the composites.
5. Among the different dual particle size combinations, 4 wt. % of large SiC particles and 2 wt. % of fine SiC particles (DPS2) composite is found to show superior wear resistance properties. This indicates that the higher amount of large size particles with a

lower amount of small size particles is the optimum combination to derive the best of both large and small sizes SiC particle effects.

References

[1] M.K. Surappa, Aluminium matrix composites: challenges and opportunities, Sadhana 28 (2003) 319–334.
[2] G.S.P. Kumar, P.G. Koppad, R. Keshavamurthy, M. Alipour, Microstructure and mechanical behaviour of in situ fabricated AA6061-TiC metal matrix composites, Arch. Civ. Mech. Eng. 17 (2017) 535–544.
[3] K.V.S. Murthy, D.P. Girish, R. Keshavamurthy, T. Varol, P.G. Koppad, Mechanical and thermal properties of AA7075/TiO_2/Fly ash hybrid composites obtained by hot forging, Prog. Nat. Sci.: Mater. Inter. 27 (2017) 474–481.
[4] H.R.A. Ram, P.G. Koppad, K.T. Kashyap, Influence of multiwalled carbon nanotubes on the aging behavior of AA 6061 alloy matrix nanocomposites, Trans. Indian Inst. Met. 67 (2014) 325–329.
[5] M. Ebrahimi, A. Zarei-Hanzaki, H.R. Abedi, M. Azimi, S.S. Mirjavadi, Correlating the microstructure to mechanical properties and wear behavior of an accumulative back extruded Al-Mg_2Si in-situ composite, Tribol. Int. 115 (2017) 199–211.
[6] J.R. Davis, Aluminium and Aluminium Alloys, ASM International, 1993, pp. 88–120.
[7] Q. Li, G.D. Zhang, J.T. Blucher, J.A. Cornie, Microstructure of the interface and interfiber regions in P-55 reinforced aluminum alloys manufactured by pressure infiltration, in: Proceedings of the Third International Conference on Composite Interfaces (ICCI-III) Held on May 21-24, 1990, pp. 131–145, in Cleveland, Ohio, USA.
[8] M. Jacquesson, A. Girard, M.-H. Vidal-sétif, R. Valle, Tensile and fatigue behavior of Al-based metal matrix composites reinforced with continuous carbon or alumina fibers: Part I. Quasi-unidirectional composites, Metall. Mater. Trans. A 35 (2004) 3289–3305.
[9] A. Bloyce, J.C. Summers, Static and dynamic properties of squeeze-cast A357-SiC particulate Duralcan metal matrix composite, Mater. Sci. Eng. A 135 (1991) 231–236.
[10] A.J. Leonard, C. Perrin, W.M. Rainforth, Microstructural changes induced by dry sliding wear of A357/SiC metal matrix composite, Mater. Sci. Technol. 13 (1997) 41–48.
[11] R. Dwivedi, G. Altland, P. Barron-Antolin, J. Leighton, T. Gillespie, Applications of Metal Matrix Composites in High Performance Racing Engines, SAE Technical Paper 911770, 1991.
[12] X. Qu, L. Zhang, M. Wu, S. Ren, Review of metal matrix composites with high thermal conductivity for thermal management applications, Prog. Nat. Sci.: Mater. Inter. 21 (2011) 189–197.
[13] Q. Zhang, G. Wu, D. Sun, G. Chen, L. Jiang, Microstructure and thermal conduction properties of an Al-12Si matrix composite reinforced with dual sized SiC particles, J. Mater. Sci. 39 (2004) 303–305.
[14] L. Avinash, T.R. Prabhu, S. Bontha, The effect on the Dry Sliding wear behavior of gravity cast A357 reinforced with dual size silicon carbide particles, Appl. Mech. Mater. 829 (2016) 83–89.
[15] S. Sharma, T. Nanda, O.P. Pandey, Effect of dual particle size (DPS) on dry sliding wear behaviour of LM30/sillimanite composites, Tribol. Int. 123 (2018) 142–154.
[16] P.N. Bindumadhavan, H.K. Wah, O. Prabhakar, Dual particle size (DPS) composites: effect on wear and mechanical properties of particulate metal matrix composites, Wear 248 (2001) 112–120.
[17] Q. Wang, F. Min, J. Zhu, Microstructure and thermo-mechanical properties of SiC_p/Al composites prepared by pressure less infiltration, J. Mater. Sci. Mater. Electron. 24 (2013) 1937–1940.
[18] S. Kumar, V. Sharma, R.S. Panwar, O.P. Pandey, Wear behavior of dual particle size (DPS) zircon sand reinforced aluminum alloy, Tribol. Lett. 47 (2012) 231–251.
[19] M. Montoya-Dávila, M.A. Pech-Canul, M.I. Pech-Canul, Effect of bi- and tri-modal size distribution on the superficial hardness of Al/SiC_p composites prepared by pressure less infiltration, Powder Technol. 176 (2007) 66–71.
[20] W. Zhou, Z.M. Xu, Casting of SiC reinforced metal matrix composites, J. Mater. Process. Technol. 63 (1–3) (1997) 358–363.
[21] J. Hashim, L. Looney, M.S.J. Hashim, Particle distribution in cast metal matrix composites - part I, J. Mater. Process. Technol. 123 (2) (2002) 251–257.
[22] J. Hashim, L. Looney, M.S.J. Hashim, Particle distribution in cast metal matrix composites - part II, J. Mater. Process. Technol. 123 (2) (2002) 258–263.
[23] S. Balasivanandha Prabu, L. Karunamoorthy, S. Kathiresan, B. Mohan, Influence of Stirring speed and stirring time on distribution of particles in cast metal matrix composites, J. Mater. Process. Technol. 171 (2) (2006) 268–273.
[24] G.S. Hanumanth, G.A. Irons, Particle incorporation by melt stirring for the production of metal-matrix composites, J. Mater. Sci. 28 (9) (1993) 2459–2465.
[25] B.M. Viswanatha, M. Prasanna Kumar, S. Basavarajappa, S. Kiran, Mechanical property evaluation of A356/SiCp/Gr metal matrix composites, J. Eng. Sci. Technol. 8 (6) (2013) 754–763.
[26] M. Shen, X. Wang, C. Li, M. Zhang, X. Hu, M. Zheng, K. Wu, Effect of bimodal size SiC Particulates on microstructure and mechanical properties of AZ31B magnesium matrix composites, Mater. Des. 52 (2013) 1011–1017.
[27] G.W. Stachowiak, A.W. Batchelor, Engineering Tribology, second ed., Butterworth- Heinemann, Boston, MA, 2001, p. 740.
[28] K.H. Zum Gahr, Microstructure and Wear of Materials, Elsevier, Amsterdam, 1987, pp. 8–17.
[29] S. Kumar, R.S. Panwar, O.P. Pandey, Effect of dual reinforced ceramic particles on high temperature tribological properties of aluminum composites, Ceram. Int. 39 (2013) 6333–6342.
[30] K.K. Ajith Kumar, Abhilash Viswanath, T.P.D. Rajan, U.T.S. Pillai, B.C. Pai, Physical, mechanical, and tribological attributes of stir-cast AZ91/SiCp composite, Acta Metall. Sin. (Engl. Lett.) 27 (2) (2014) 295–305.
[31] K. Deng, J. Shi, C. Wang, X. Wang, Y. Wu, K. Nie, K. Wu, Microstructure and strengthening mechanism of bimodal size particle reinforced magnesium matrix composite, Composite Part A 43 (2012) 1280–1284.
[32] K.K. Deng, K. Wu, Y.W. Wu, K.B. Nie, M.Y. Zheng, Effect of submicron size SiC particulates on microstructure and mechanical properties of AZ91 magnesium matrix composites, J. Alloy. Comp. 504 (2010) 542.
[33] A. Sanaty-Zadeh, P.K. Rohatgi, Corrigendum to: comparison between current models for the strength of particulate-reinforced metal matrix nanocomposites with emphasis on consideration of Hall–Petch effect, Mater. Sci. Eng. A 531 (2012) 112–118.
[34] Naveen K. Mahenderkar, T. Ram Prabhu, Anil Kumar, Nanocomposites Potential for Aero Applications, in: Indian Institute of Metals Series, vol. 1, Springer, 2016, pp. 391–411.
[35] K.R. Suresh, H.B. Niranjan, P. Martin Jebaraj, M.P. Chowdiah, Tensile and wear properties of aluminium composites, Wear 225 (2003) 638–642.
[36] T Ram Prabhu, Effect of bimodal size particles reinforcement on the wear, friction and mechanical properties of brake composites, Tribol. Mater. Surface Interfac., (10) 4, 163-171.
[37] G.E. Dieter, Mechanical Metallurgy, third ed., Mc Graw-Hill Book Co., New York, 1986. XXIII+751 p., DM 138.50, ISBN 0-07-016893-3.
[38] A. Ahmed, A.J. Neely, K. Shankar, Experimental comparison of the effects of nanometric and micrometric particulates on the tensile properties and fracture behavior of Al Composites at room and elevated temperatures, Metall. Mater. Trans. 42 (2011) 795–815.
[39] Z. Chen, X. Hao, Y. Wang, K. Zhao, In-situ observation of tensile fracture in A357 casting alloys, J. Mater. Sci. Technol. 30 (2014) 139–145.
[40] W. Jiang, Z. Fan, Y. Dai, C. Li, Effects of rare earth elements addition on microstructures, tensile properties and fractography of A357 alloy, Mater. Sci. Eng. A 597 (2014) 237–244.
[41] M.L. Ted Guo, Chi-Y.A. Tsao, Tribological behavior of aluminum/SiC/nickel-coated graphite hybrid composites, Mater. Sci. Eng. A 333 (2002) 134–145.
[42] B.K. Show, D.K. Mondal, J. Maity, Wear behavior of a novel aluminum-based hybrid composite, Metall. Mater. Trans. A 45 (2014) 1027–1040.
[43] R.N. Rao, S. Das, Wear coefficient and reliability of sliding wear test procedure for high strength aluminium alloy and composite, Mater. Des. 31 (2010) 3227–3233.
[44] R.L. Deuis, C. Subramanian, J.M. Yellup, Dry sliding wear of aluminium composites - a review, Compos. Sci. Technol. 57 (1997) 415–435.
[45] T.R. Prabhu, V.K. Varma, S. Vedantam, Effect of SiC volume fraction and size on dry sliding wear of Fe/SiC/Graphite hybrid composites for high sliding speed applications, Wear 309 (2014) 1–10.
[46] T.R. Prabhu, V.K. Varma, S. Vedantam, Effect of reinforcement type, size, and volume fraction on the tribological behavior of Fe matrix composites at high sliding speed conditions, Wear 309 (2014) 247–255.
[47] R.N. Rao, S. Das, Wear coefficient and reliability of sliding wear test procedure for high strength aluminium alloy and composite, Mater. Des. 31 (2010) 3227–3233.
[48] D.K. Dwivedi, T.S. Arjun, P. Thakur, H. Vaidya, K. Singh, Sliding wear and friction behaviour of Al–18% Si–0.5% Mg alloy, J. Mater. Process. Technol. 152 (2004) 323–328.
[49] S.K. Biswas, B.N. Pramila Bai, Dry wear of aluminium graphite particle composites, Wear 68 (1981) 347–358.
[50] R.N. Rao, S. Das, Effect of sliding distance on the wear and friction behavior of as cast and heat-treated Al–SiCp composites, Mater. Des. 32 (2011) 3051–3058.
[51] R.N. Rao, S. Das, Effect of SiC content and sliding speed on the wear behaviour of aluminium matrix composites, Mater. Des. 32 (2011) 1066–1071.
[52] V. Sharma, S. Kumar, R.S. Panwar, O.P. Pandey, Microstructural and wear behavior of dual reinforced particle (DRP) aluminum alloy composite, J. Mater. Sci. 47 (2012) 6633–6646.
[53] T. Rajmohan, K. Palanikumar, S. Ranganathan, Evaluation of mechanical and wear properties of hybrid aluminium matrix composites, Trans. Nonferrous Metals Soc. China 23 (2013) 2509–2517.
[54] M. Uthayakumar, S. Aravindan, K. Rajkumar, Wear performance of Al–SiC–B_4C hybrid composites under dry sliding conditions, Mater. Des. 47 (2013) 456–464.